OPTIMAL CONTROL APPLICATIONS AND METHODS
Optim. Control Appl. Meth. 2010; **31**:433–449
Published online 27 September 2010 in Wiley Online Library (wileyonlinelibrary.com). DOI: 10.1002/oca.959

Worst-case analysis of distributed parameter systems with application to the 2D reaction–diffusion equation‡

Masako Kishida and Richard D. Braatz*, †

University of Illinois at Urbana-Champaign, 1206 W. Green Street, Urbana, IL 61801-2906, U.S.A.

SUMMARY

It is well known that optimal control trajectories can be highly sensitive to perturbations in the model parameters. Computationally efficient numerical algorithms are presented for the worst-case analysis of the effects of parametric uncertainties on boundary control problems for finite-time distributed parameter systems. The approach is based on replacing the full-order model of the system with a power series expansion that is analyzed by linear matrix inequalities or power iteration, which are polynomial-time algorithms. Theory and algorithms are provided for computing the most positive and most negative worst-case deviation in a state or output, in contrast to the 'two-sided' deviations normally computed in worst-case analyses. Application to the Dirichlet boundary control of the reaction–diffusion equation to track a desired two-dimensional concentration field illustrates the promise of the approach. Copyright © 2010 John Wiley & Sons, Ltd.

Received 29 April 2010; Revised 6 July 2010; Accepted 6 July 2010

KEY WORDS: distributed parameter systems; boundary control; robustness analysis; partial differential equations

1. INTRODUCTION

The boundary control of distributed parameter systems (DPS) has received increased interest in the recent years for a wide range of applications in mechanical, chemical, and biomedical engineering [2, 3], including microchemical systems [4], tissue engineering [5], and glass cooling [6]. While the analysis of the effects of parametric uncertainties is well established for lumped parameter systems (e.g. see [7–9]), the field is much less mature for DPS. The three most popular classes of uncertainty analysis approaches for DPS discussed in the control literature are based on (1) application of the Monte Carlo method to the full simulation code (e.g., [10]), (2) running the full simulation code for all parameters obtained by gridding the parameter space (e.g. [10]), and (3) Lyapunov functions (e.g. [11]). The first two classes of numerical algorithms can produce robustness margins with a low level of conservatism but are computationally expensive for problems with multiple spatial dimensions and parameters. For example, using a relatively coarse grid of 10 points per parameter requires $10^{\dim(p)}$ runs of the full simulation code, where

*Correspondence to: Richard D. Braatz, 293 Roger Adams Laboratory, Box C-3 600 South Mathews Avenue, Urbana, IL 61801-3602, U.S.A.
†E-mail: braatz@illinois.edu
‡This manuscript is a significantly expanded and revised version of a manuscript presented at the Eighteenth International Symposium on Mathematical Theory of Networks and Systems [1].

p is the vector of uncertain parameters. This is computationally feasible only for systems with a small number of parameters. The third class of robustness analysis methods for DPS is not always computationally expensive but apply only to specific control structures and/or is conservative.

This paper describes the use of power series expansions and structured singular value analysis for worst-case analysis of the effects of uncertainties on boundary control problems for finite-time DPS. The approach is based on the same philosophy as polynomial chaos and power series expansions applied in the environmental field [12], which is to first compute an approximation to the full simulation model, followed by application of robustness analysis to the approximate model. The very low computational cost of the approximate model enables the application of the Monte Carlo method or gridding the parameter space, as in methods (1) and (2) above, as well as the application of polynomial-time norm-based analytical methods as applied here, which include the application of linear matrix inequalities (LMIs) to compute tight upper bounds and power iteration to compute lower bounds on the worst-case deviations of the states and control objectives. A novel contribution is the derivation of theory and algorithms for computing the most positive and most negative worst-case deviation in a state or output, in contrast to the 'two-sided' deviations normally computed in worst-case analyses. The proposed approach is illustrated by application to a boundary control problem for a reaction–diffusion equation with two spatial dimensions.

2. WORST-CASE ANALYSIS

The proposed approach for worst-case robustness analysis of finite-time DPS is to first approximate the original partial differential equation (PDE) by a power series expansion and then apply polynomial-time analysis tools developed for providing tight bounds on the worst-case deviations for such expansions [13–15]. To simplify the presentation, model parameter uncertainties and implementation biases in the boundary control inputs will be collectively referred to as 'uncertainties' and collected into a single vector $\delta\lambda$, which is related to the vector of uncertain variables λ and the vector of nominal values λ_{nom} by

$$\lambda := \lambda_{\text{nom}} + \delta\lambda. \tag{1}$$

The uncertainty set is described by

$$E_\lambda = \{\lambda : \lambda = \lambda_{\text{nom}} + \delta\lambda, \|W\delta\lambda\|_{\text{r}} \leqslant 1\}, \tag{2}$$

where W is a specified positive-definite weighting matrix and $\|\cdot\|_{\text{r}}$ is any well-defined norm. For the case where the set of λ contains time-invariant vectors, examples of such norms are the Hölder 1-, 2-, and ∞-norms. For the 2-norm, the uncertainty set is described by a hyperellipsoid. An uncertainty set described by independent upper and lower bounds on each parameter

$$E_\lambda = \{\lambda : \lambda = \hat{\lambda}_{\text{nom}} + \delta\hat{\lambda}, \delta\underline{\lambda} \leqslant \delta\hat{\lambda} \leqslant \delta\bar{\lambda}\}, \tag{3}$$

where the vectors $\delta\underline{\lambda}$ and $\delta\bar{\lambda}$ are the lower and upper bounds on the vector of uncertainties, can be rewritten in terms of (2) for $r = \infty$ by specifying[§]

$$W_{ii} = \frac{2}{\delta\bar{\lambda}_i - \delta\underline{\lambda}_i}, \quad W_{ij} = 0 \ \ \forall i \neq j, \tag{4}$$

$$\lambda_{\text{nom}} = \hat{\lambda}_{\text{nom}} + \tfrac{1}{2}(\delta\bar{\lambda} + \delta\underline{\lambda}). \tag{5}$$

[§] $\delta\bar{\lambda}_i \neq \delta\underline{\lambda}_i$ for all i because λ is an uncertain vector.

DOI: 10.1002/oca

While only a single norm is treated here to simplify the notation, the results can be generalized to the case in which different norms are specified for different sets of elements of λ. This would be useful, for example, if the uncertainties associated with some variables lie within a hyperellipsoidal uncertainty set whereas the uncertainties of other variables lie within lower and upper bounds on each variable.

The worst-case positive and negative deviations due to uncertainties are defined by

$$\delta\bar{y}_{\text{w.c.}} := \max_{\lambda \in E_\lambda} \{y(\lambda) - y(\hat{\lambda}_{\text{nom}})\} \tag{6}$$

and

$$\delta\underline{y}_{\text{w.c.}} := \min_{\lambda \in E_\lambda} \{y(\lambda) - y(\hat{\lambda}_{\text{nom}})\}, \tag{7}$$

where y is a state or output at a particular time t of interest. In general, solving these optimizations is NP-hard [16, 17] and is especially computationally expensive for DPS. This optimization can be greatly simplified, however, by inserting a power series expansion of finite order for y into (6) and (7), for which tight bounds on the worst-case deviation in y and an estimate for a worst-case uncertainty vector can be computed using dual norms, LMI, or power iteration. This approach also applies to any sufficiently smooth function of the states or control objectives.

The power series expansion only needs to be an accurate representation for y within the trajectory bundle defined by the uncertainty description, and does not need to be an accurate representation for the entire state space. This enables the use of fairly low-order expansions to obtain an accurate estimate of worst-case deviation, with low computational cost. The remainder of this section presents specific expressions for robust analysis for first- and second-order expansions, and the procedure for higher-order expansions.

2.1. First-order series expansion

Define the first-order expansion written in terms of deviation variables as

$$\delta y_1 := M\delta\lambda \approx y(\lambda) - y(\lambda_{\text{nom}}), \tag{8}$$

where

$$M_i := \left.\frac{\partial y}{\partial \lambda_i}\right|_{\lambda=\lambda_{\text{nom}}}, \tag{9}$$

provided that y is differentiable in λ. The optimization (6) with this first-order expansion used in the objective can be solved analytically for a wide variety of norms including all of the Hölder norms. For example, for the ∞-norm the solution is

$$\max_{\|W\delta\lambda\|_\infty \leqslant 1} \delta y_1 = \max_{\|W\delta\lambda\|_\infty \leqslant 1} M\delta\lambda = \max_{\|W\delta\lambda\|_\infty \leqslant 1} |M\delta\lambda| = \|MW^{-1}\|_1, \tag{10}$$

which is a standard result for dual norms. A worst-case uncertainty vector is[¶]

$$\delta\lambda_{\text{w.c.}} = W^{-1}e, \tag{11}$$

where

$$e_i = \frac{(MW^{-1})_i}{|(MW^{-1})_i|}. \tag{12}$$

[¶]This vector is not necessarily unique.

DOI: 10.1002/oca

with this worst-case uncertainty vector, the first-order estimate of the maximum worst-case deviation in y is

$$\delta\bar{y}_{1,\text{w.c.}} = M\delta\lambda_{\text{w.c.}} = \sum_i |(MW^{-1})_i|. \tag{13}$$

The first-order estimate of the minimum worst-case deviation in y is

$$\delta\underline{y}_{1,\text{w.c.}} = -M\delta\lambda_{\text{w.c.}} = -\sum_i |(MW^{-1})_i|, \tag{14}$$

which is obtained by using $-\delta\lambda_{\text{w.c.}}$ for the worst-case uncertainty vector.

2.2. Second- and higher-order expansions

Similarly, define the second-order expansion as

$$\delta y_2 := M\delta\hat{\lambda} + \delta\hat{\lambda}^{\mathrm{T}} H \delta\hat{\lambda} \approx y(\lambda) - y(\hat{\lambda}_{\text{nom}}), \tag{15}$$

where

$$M_i := \left.\frac{\partial y}{\partial \lambda_i}\right|_{\lambda=\hat{\lambda}_{\text{nom}}}, \tag{16}$$

and

$$H_{ij} := \left.\frac{1}{2}\frac{\partial^2 y}{\partial\lambda_i \partial\lambda_j}\right|_{\lambda=\hat{\lambda}_{\text{nom}}}, \tag{17}$$

for any doubly differentiable function. The second-order estimates of the maximum and minimum worst-case deviations in y are

$$\delta\bar{y}_{2,\text{w.c.}} := \max_{\delta\hat{\lambda}} \delta y_2, \tag{18}$$

$$\delta\underline{y}_{2,\text{w.c.}} := \min_{\delta\hat{\lambda}} \delta y_2, \tag{19}$$

subject to the constraint (3).

The estimates can be written in terms of the mixed structured singular value μ [16]. For any real k,

$$\max_{\delta\underline{\lambda}\leqslant\delta\hat{\lambda}\leqslant\delta\bar{\lambda}} |\delta y_2| = \max_{\delta\underline{\lambda}\leqslant\delta\hat{\lambda}\leqslant\delta\bar{\lambda}} |M\delta\hat{\lambda} + \delta\hat{\lambda}^{\mathrm{T}} H\delta\hat{\lambda}| \geqslant k \Longleftrightarrow \mu_\Delta(N) \geqslant k, \tag{20}$$

where

$$N := \begin{bmatrix} 0 & 0 & kw \\ kH & 0 & kHz \\ z^{\mathrm{T}}H + M & w^{\mathrm{T}} & z^{\mathrm{T}}Hz + Mz \end{bmatrix}, \tag{21}$$

$$w := \tfrac{1}{2}(\delta\bar{\lambda} - \delta\underline{\lambda}), \quad z := \tfrac{1}{2}(\delta\bar{\lambda} + \delta\underline{\lambda}), \tag{22}$$

DOI: 10.1002/oca

the perturbation block $\Delta = \mathrm{diag}(\Delta_r, \Delta_r, \delta_c)$, Δ_r consists of independent real scalars, and δ_c is a complex scalar. This implies that

$$\max_{\delta\underline{\lambda} \leqslant \delta\hat{\lambda} \leqslant \delta\bar{\lambda}} |\delta y_2| = \max_{\mu_\Delta(N) \geqslant k} k := k_\Delta \tag{23}$$

where the right-hand side can be computed from a single skewed mixed structured singular value calculation [18]. The worst-case perturbation vector determines whether the perturbation $\delta\lambda$ that achieves the maximum in

$$\max_{\delta\underline{\lambda} \leqslant \delta\hat{\lambda} \leqslant \delta\bar{\lambda}} |\delta y_2| \tag{24}$$

produces a positive or negative δy_2, which corresponds to $\delta\bar{y}_{2,\mathrm{w.c.}}$ or $\delta\underline{y}_{2,\mathrm{w.c.}}$, respectively. If the δy_2 computed by insertion of this worst-case perturbation into the quadratic equation is positive,

$$\delta\bar{y}_{2,\mathrm{w.c.}} = k_\Delta, \tag{25}$$

define

$$\delta\tilde{y}_2 := \delta y_2 - k_\Delta, \tag{26}$$

then

$$\max_{\delta\underline{\lambda} \leqslant \delta\hat{\lambda} \leqslant \delta\bar{\lambda}} |\delta\tilde{y}_2| = \max_{\mu_\Delta(\tilde{N}) \geqslant \tilde{k}} \tilde{k} := \tilde{k}_\Delta, \tag{27}$$

where

$$\tilde{N} := \begin{bmatrix} 0 & 0 & \tilde{k}w \\ \tilde{k}H & 0 & \tilde{k}Hz \\ z^{\mathrm{T}}H + M & w^{\mathrm{T}} & z^{\mathrm{T}}Hz + Mz - k_\Delta \end{bmatrix}. \tag{28}$$

That $\delta\tilde{y}_2$ can take any value in the interval

$$[\delta\underline{y}_{2,\mathrm{w.c.}} - k_\Delta, 0], \tag{29}$$

which implies that

$$\tilde{k}_\Delta = -\delta\underline{y}_{2,\mathrm{w.c.}} + k_\Delta \tag{30}$$

and

$$\delta\underline{y}_{2,\mathrm{w.c.}} = k_\Delta - \tilde{k}_\Delta \tag{31}$$

so that both the minimum and maximum perturbations in y_2 are determined.

If the δy_2 computed by insertion of the worst-case perturbation from (23) into the quadratic equation is negative,

$$\delta\underline{y}_{2,\mathrm{w.c.}} = -k_\Delta, \tag{32}$$

define

$$\delta\hat{y}_2 := \delta y_2 + k_\Delta, \tag{33}$$

DOI: 10.1002/oca

then

$$\max_{\delta\underline{\lambda}\leqslant\delta\hat{\lambda}\leqslant\delta\bar{\lambda}} |\delta\hat{y}_2| = \max_{\mu_\Delta(\hat{N})\geqslant\hat{k}} \hat{k} := \hat{k}_\Delta, \tag{34}$$

where

$$\hat{N} := \begin{bmatrix} 0 & 0 & \hat{k}w \\ \hat{k}H & 0 & \hat{k}Hz \\ z^{\mathrm{T}}H+M & w^{\mathrm{T}} & z^{\mathrm{T}}Hz+Mz+k_\Delta \end{bmatrix}. \tag{35}$$

That $\hat{y}_2$ can take any value in the interval

$$[0, \delta\bar{y}_{2,\mathrm{w.c.}}+k_\Delta], \tag{36}$$

which implies that

$$\hat{k}_\Delta = \delta\bar{y}_{2,\mathrm{w.c.}}+k_\Delta \tag{37}$$

and

$$\delta\bar{y}_{2,\mathrm{w.c.}} = \hat{k}_\Delta - k_\Delta, \tag{38}$$

indicating again that the minimum and maximum values for y_2 can be computed from two skewed mixed structured singular value calculations.

An alternative approach can be derived based on an *a priori* upper bound c on $|\delta y_2|$ over (3). Such an upper bound can be determined using the relation

$$\delta\hat{\lambda} = \lambda_{\mathrm{nom}} - \hat{\lambda}_{\mathrm{nom}} + \delta\lambda \tag{39}$$

and applying some standard results from linear algebra:

$$\max_{\delta\underline{\lambda}\leqslant\delta\hat{\lambda}\leqslant\delta\bar{\lambda}} |M\delta\hat{\lambda}+\delta\hat{\lambda}^{\mathrm{T}}H\delta\hat{\lambda}| \tag{40}$$

$$= \max_{\|W\delta\lambda\|_\infty\leqslant 1} |M(\lambda_{\mathrm{nom}}-\hat{\lambda}_{\mathrm{nom}}+\delta\lambda)+(\lambda_{\mathrm{nom}}-\hat{\lambda}_{\mathrm{nom}}+\delta\lambda)^{\mathrm{T}}H(\lambda_{\mathrm{nom}}-\hat{\lambda}_{\mathrm{nom}}+\delta\lambda)| \tag{41}$$

$$= \max_{\|W\delta\lambda\|_\infty\leqslant 1} |M(\lambda_{\mathrm{nom}}-\hat{\lambda}_{\mathrm{nom}})+(\lambda_{\mathrm{nom}}-\hat{\lambda}_{\mathrm{nom}})^{\mathrm{T}}H(\lambda_{\mathrm{nom}}-\hat{\lambda}_{\mathrm{nom}})+(M+2(\lambda_{\mathrm{nom}}-\hat{\lambda}_{\mathrm{nom}})^{\mathrm{T}}H+\delta\lambda^{\mathrm{T}}H)\delta\lambda| \tag{42}$$

$$\leqslant |M(\lambda_{\mathrm{nom}}-\hat{\lambda}_{\mathrm{nom}})+(\lambda_{\mathrm{nom}}-\hat{\lambda}_{\mathrm{nom}})^{\mathrm{T}}H(\lambda_{\mathrm{nom}}-\hat{\lambda}_{\mathrm{nom}})| + \max_{\|W\delta\lambda\|_\infty\leqslant 1} |(M+2(\lambda_{\mathrm{nom}}-\hat{\lambda}_{\mathrm{nom}})^{\mathrm{T}}H+\delta\lambda^{\mathrm{T}}H)\delta\lambda| \tag{43}$$

$$\leqslant |M(\lambda_{\mathrm{nom}}-\hat{\lambda}_{\mathrm{nom}})+(\lambda_{\mathrm{nom}}-\hat{\lambda}_{\mathrm{nom}})^{\mathrm{T}}H(\lambda_{\mathrm{nom}}-\hat{\lambda}_{\mathrm{nom}})| + \max_{\|W\delta\lambda\|_\infty\leqslant 1} \|(M+2(\lambda_{\mathrm{nom}}-\hat{\lambda}_{\mathrm{nom}})^{\mathrm{T}}H+\delta\lambda^{\mathrm{T}}H)W^{-1}\|_1 := c, \tag{44}$$

where the latter optimization can be solved in polynomial-time by linear programming. For such an upper bound c,

$$\delta\overline{y}_{2,\mathrm{w.c.}}+c = \max_{\delta\underline{\lambda}\leqslant\delta\hat{\lambda}\leqslant\delta\bar{\lambda}} \delta y_2 + c \geqslant k_{\mathrm{c}} \Longleftrightarrow \mu_\Delta(N_{\mathrm{c}}) \geqslant k_{\mathrm{c}}, \tag{45}$$

DOI: 10.1002/oca

where

$$N_c := \begin{bmatrix} 0 & 0 & k_c w \\ k_c H & 0 & k_c H z \\ z^T H + M & w^T & z^T H z + M z + c \end{bmatrix}, \tag{46}$$

and the maximum positive value for δy_2 can be computed from

$$\delta \bar{y}_{2,\text{w.c.}} = \max_{\mu_\Delta(N_c) \geqslant k_c} k_c - c. \tag{47}$$

Similarly, selecting a negative c with high enough magnitude to ensure that $\delta y_2 + c < 0$‖ results in

$$\delta \underline{y}_{2,\text{w.c.}} = - \max_{\mu_\Delta(N_c) \geqslant k_c} k_c - c. \tag{48}$$

A polynomial-time upper bound for the calculation of the skewed mixed structured singular value and a corresponding worst-case perturbation can be computed using LMIs [19]. This upper bound is often tight for practical problems, and can be complemented with a polynomial-time lower bound computed by a power iteration [20] to assess conservatism. The advantage of the above k_Δ procedure for computing $\delta \underline{y}_{2,\text{w.c.}}$ and $\delta \bar{y}_{2,\text{w.c.}}$ is that the approach does not introduce a potentially large number c into the matrix in the skewed mixed structured singular value calculation. The advantage of the c procedure is that lower and upper bounds in the skewed mixed structured singular value calculation directly translate into lower and upper bounds on $\underline{y}_{2,\text{w.c.}}$ and $\bar{y}_{2,\text{w.c.}}$ via (47) and (48). This translation is messier for the k_Δ procedure (details are not shown for brevity).

Higher-order approximations and other norms on the uncertainty set (2) can be computed by using multi-dimensional realization algorithms (e.g. [21]) and the generalized-norm structured singular value (e.g., [22]), respectively.**

The above theory and numerical algorithms can be used to evaluate the feasibility of nonlinear constraints in the presence of model uncertainties:

$$g(\mathbf{a}, \lambda) < 0 \quad \forall \lambda \in E_\lambda, \tag{49}$$

where $\mathbf{a}$ is a vector of optimization variables used to parameterize the control input u. This robust feasibility constraint (49) can be written as

$$\max_{\lambda \in E_\lambda} g(\mathbf{a}, \lambda) < 0. \tag{50}$$

The numerical algorithms can be used to compute tight polynomial-time bounds on the worst-case upper bound on g, which can be compared with zero to assess whether the nonlinear constraint (49) holds for all uncertainty vectors λ within the uncertainty set E_λ. Steady-state or dynamic feasibility can be assessed, depending on whether g is defined for a steady-state or for each time t. These algorithms can be used to compute backoff terms from a nominal optimal solution to ensure feasibility of the constraints, which generalizes the first- and second-order methods that have been described in the literature [23–25]. Alternatively, the LMI upper bound for each feasibility condition of the form (50) can be included into robust optimal control design, which replaces all of the NP-hard robust feasibility constraints with convex LMI constraints. The dependency of the optimization objective and constraints on $\mathbf{a}$ could

‖For example, selecting c equal to negative value in (44) will work.
**These approaches also enable the use of rational approximations.

DOI: 10.1002/oca

still be nonconvex, but each inner maximization (50) would be replaced by a convex constraint. This approach to ensuring robust feasibility is more direct than introducing backoff terms (e.g. see discussion by Glemmestad *et al.* [26] and Govatsmark and Skogestad [27]).

While a power-series expansion is used to obtain bounds on the worst-case deviations, a polynomial chaos expansion can be used for a stochastic processes to replace the full-order model of the system and to obtain estimate of its stochastic deviations in a similar manner.

3. BOUNDARY CONTROL PROBLEM

The remainder of this paper illustrates this robustness analysis approach for the boundary control of the DPS:

$$\frac{\partial C}{\partial t} = D\left(\frac{\partial^2 C}{\partial x^2} + \frac{\partial^2 C}{\partial y^2}\right) - kC, \tag{51}$$

with boundary conditions

$$\begin{aligned} C(0,y,t) &= u_{x0}(y,t), \quad C(1,y,t) = u_{x1}(y,t), \\ C(x,0,t) &= u_{y0}(x,t), \quad C(x,1,t) = u_{y1}(x,t), \end{aligned} \tag{52}$$

and zero initial condition

$$C(x,y,0) = 0. \tag{53}$$

This parabolic PDE describes the concentration or temperature field C for a reacting solid with mass or heat transfer occurring via molecular motion (diffusion or thermal conduction, respectively), where D is the diffusion coefficient and k is the reaction rate constant. The control objective is to find feasible boundary control inputs

$$u(x,y,t) = [u_{x0}(y,t)\ \ u_{x1}(y,t)\ \ u_{y0}(x,t)\ \ u_{y1}(x,t)]^{\mathrm{T}} \tag{54}$$

that produce a field $C(x,y,t)$ that is as close as possible to a reference field $R(x,y,t)$,

$$\min_{u\in\mathscr{U}} \int_0^{t_f}\int_0^1\int_0^1 (R(x,y,t) - C(x,y,t))^2 \,\mathrm{d}x\,\mathrm{d}y\,\mathrm{d}t, \tag{55}$$

where $\mathscr{U}$ is the domain of the optimization variable $u(x,y,t)$ (sometimes this constraint is necessary to ensure that the boundary control inputs are physically implementable).

4. OPTIMAL CONTROL DESIGN

With the boundary control trajectories parameterized in terms of the eigenfunctions of the PDE (51) in space and Heaviside step functions S in time,

$$\begin{aligned} u_{x0}(y,t) &= \sum_{i=1}^{I}\sum_{j=1}^{J} a_{x0ij} \sin i\pi y\ S(t-\tau_j), \quad u_{x1}(y,t) = \sum_{i=1}^{I}\sum_{j=1}^{J} a_{x1ij} \sin i\pi y\ S(t-\tau_j), \\ u_{y0}(x,t) &= \sum_{i=1}^{I}\sum_{j=1}^{J} a_{y0ij} \sin i\pi x\ S(t-\tau_j), \quad u_{y1}(x,t) = \sum_{i=1}^{I}\sum_{j=1}^{J} a_{y1ij} \sin i\pi x\ S(t-\tau_j), \end{aligned} \tag{56}$$

DOI: 10.1002/oca

the solution to the PDE is

$$C(x,y,t)=\mathbf{a}^{\mathrm{T}}\mathbf{C}, \tag{57}$$

where

$$\mathbf{a}=\begin{bmatrix} a_{x011}\\ \vdots\\ a_{x01J}\\ a_{x021}\\ \vdots\\ a_{x0IJ}\\ a_{x111}\\ \vdots\\ a_{x1IJ}\\ a_{y011}\\ \vdots\\ a_{y0IJ}\\ a_{y111}\\ \vdots\\ a_{y1IJ}\end{bmatrix},\quad \mathbf{C}=\begin{bmatrix} C_{x011}(x,y,t)\\ \vdots\\ C_{x01J}(x,y,t)\\ C_{x021}(x,y,t)\\ \vdots\\ C_{x0IJ}(x,y,t)\\ C_{x111}(x,y,t)\\ \vdots\\ C_{x1IJ}(x,y,t)\\ C_{y011}(x,y,t)\\ \vdots\\ C_{y0IJ}(x,y,t)\\ C_{y111}(x,y,t)\\ \vdots\\ C_{y1IJ}(x,y,t)\end{bmatrix}, \tag{58}$$

and each element of $\mathbf{C}$ corresponds to the solution to the PDE with its corresponding element of $\mathbf{a}$ equal to 1 with all other entries equal to zeros. With $\mathscr{U}$ defined as the constraint that the control input is nonnegative, substituting (57) into the objective function (55) gives

$$\min_{\substack{\mathbf{a}\\ u(x,y,t)\geqslant 0}} \int_0^{t_f}\int_0^1\int_0^1 (R(x,y,t)-\mathbf{a}^{\mathrm{T}}\mathbf{C})^2\,\mathrm{d}x\,\mathrm{d}y\,\mathrm{d}t, \tag{59}$$

which has the same solution as the nonlinear program

$$\min_{\substack{-Q(x,y)\mathbf{a}\leqslant 0\\ 0\leqslant x\leqslant 1\\ 0\leqslant y\leqslant 1}} \tfrac{1}{2}\mathbf{a}^{\mathrm{T}}\mathbf{G}\mathbf{a}+\mathbf{f}^{\mathrm{T}}\mathbf{a}, \tag{60}$$

DOI: 10.1002/oca

where

$$\mathbf{G} = \int_0^{t_f} \int_0^1 \int_0^1 \mathbf{C}\mathbf{C}^{\mathrm{T}} \,\mathrm{d}x \,\mathrm{d}y \,\mathrm{d}t, \tag{61}$$

$$\mathbf{f} = -\int_0^{t_f} \int_0^1 \int_0^1 R(x, y, t)\mathbf{C}^{\mathrm{T}} \,\mathrm{d}x \,\mathrm{d}y \,\mathrm{d}t, \tag{62}$$

$$Q(x, y) = \mathrm{diag}(v_x, v_x, v_y, v_y), \tag{63}$$

v_x is a row vector collecting $\sin i\pi y \;\; S(t-\tau_j)$, and v_y is a row vector collecting $\sin i\pi x \;\; S(t-\tau_j)$ for $i=1,\ldots,I$ and $j=1,\ldots,J$. This nonlinear program can be approximately solved to any degree of accuracy as a quadratic program with linear constraints by replacing the constraints by the finite set of linear inequalities that results from evaluating the nonlinear inequality constraint for a fine mesh of (x, y) points over the spatial domain. The significant increase in the number of inequality constraints is offset by the ready availability of very efficient software for solving quadratic programs with large numbers of linear inequality constants. For the case of no constraints, the optimal control inputs are parameterized by

$$\mathbf{a} = -\mathbf{G}^{-1}\mathbf{f}, \tag{64}$$

with the optimal field being

$$C_{\mathrm{opt}}(x, y, t) = -(\mathbf{G}^{-1}\mathbf{f})^{\mathrm{T}}\mathbf{C}. \tag{65}$$

For analysis of the worst-case deviations in the optimal C, the perturbations in the uncertain variables are

$$\delta\lambda = [\delta D \;\; \delta k \;\; \delta u_{x0} \;\; \delta u_{x1} \;\; \delta u_{y0} \;\; \delta u_{y1}]^{\mathrm{T}}, \tag{66}$$

where the last four elements are time-invariant additive errors on the four boundary control trajectories.

5. NUMERICAL EXAMPLE

5.1. Optimal control design

Let the reference field

$$R(x, y, t) = (\mathrm{e}^{-x} - \mathrm{e}^{-3x})(\mathrm{e}^{-y} - \mathrm{e}^{-4y})(\mathrm{e}^{-t} - \mathrm{e}^{-2t}) \tag{67}$$

with the dimensionless constants $D=1$ and $k=7.6$, and the boundary control of the form

$$\begin{aligned} u_{x0}(y,t) &= \sum_{i=1}^{5}\sum_{j=1}^{5} a_{x0ij} \sin i\pi y \;\; S(t-\tau_j), \quad u_{x1}(y,t) = \sum_{i=1}^{5}\sum_{j=1}^{5} a_{x1ij} \sin i\pi y \;\; S(t-\tau_j), \\ u_{y0}(x,t) &= \sum_{i=1}^{5}\sum_{j=1}^{5} a_{y0ij} \sin i\pi x \;\; S(t-\tau_j), \quad u_{y1}(x,t) = \sum_{i=1}^{5}\sum_{j=1}^{5} a_{y1ij} \sin i\pi x \;\; S(t-\tau_j), \end{aligned} \tag{68}$$

DOI: 10.1002/oca

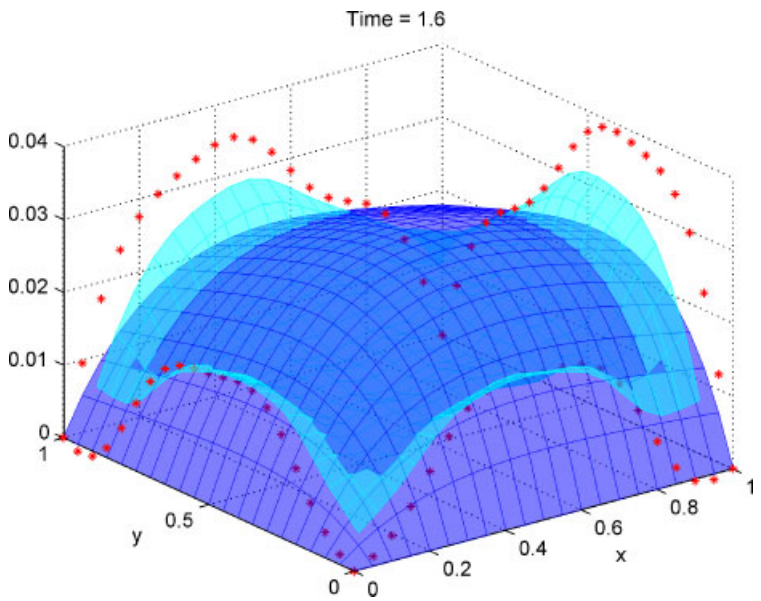

Figure 1. Reference $R(x, y, t)$ (dark blue) and optimal $C_{\text{opt}}(x, y, t)$ (light cyan) fields at $t = 1.6$. The red asterisks are the boundary control inputs at $t = 1.6$ (the values for C_{opt} on the boundary are the same as the asterisks). Refer online version for interpretation of color.

where $\{\tau_1, \ldots, \tau_5\} = \{0.5, 1.0, 1.5, 2.0, 2.5\}$ and there are no constraints on u for simplicity.[††] The boundary control problem is to determine the optimal values of $a_{x0ij}, a_{x1ij}, a_{y0ij}$, and a_{y1ij} for $i, j = 1, \ldots, 5$. The reference field and output field obtained by optimal boundary controls are shown in Figure 1. At this particular time instance, the optimal concentration field is mostly higher than the reference field near the boundaries and lower in the interior.

5.2. *Robustness analysis*

Consider upper and lower bounds on the uncertain variables (66) as

$$\delta\bar{\lambda} = [0.1 \;\; 1 \;\; 0.001 \;\; 0.001 \;\; 0.001 \;\; 0.001]^{\mathrm{T}}, \tag{69}$$

$$\delta\underline{\lambda} = -\delta\bar{\lambda}. \tag{70}$$

This uncertainty set is equivalent to (2) with the weight matrix

$$W = \mathrm{diag}(10, 1, 1000, 1000, 1000, 1000), \tag{71}$$

and $r = \infty$. For this example, M and H can be obtained analytically from the solution of the PDE obtained by separation of variables or the Fourier series method.

[††] An example of a boundary control problem in which the constraints could probably be dropped is for a first-order reversible reaction occurring in a solid with high equilibrium value for the concentration, in which case (51) would be written in terms of deviations from the equilibrium concentration.

DOI: 10.1002/oca

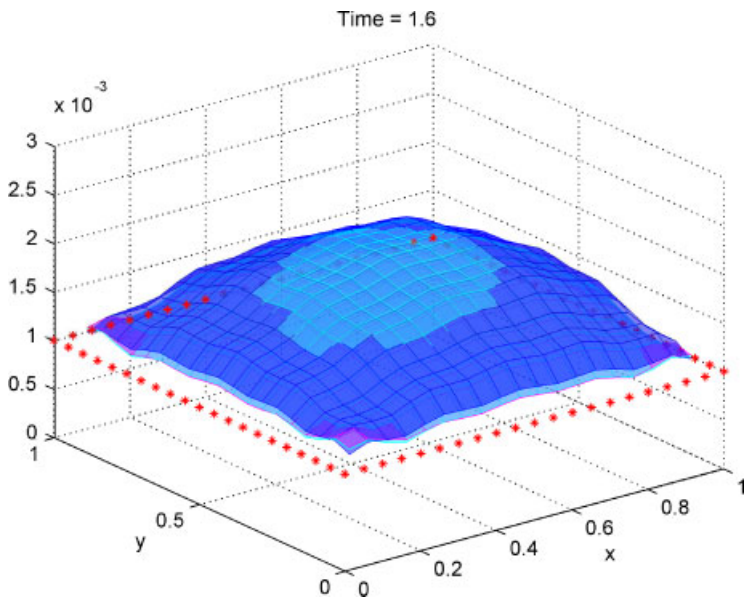

Figure 2. Maximum positive deviations in the controls δu (asterisks) and the concentration fields (surface meshes) due to uncertainties estimated by δC_{ep} (magenta), $\delta C_{1,\mathrm{ep}}$ (blue), and $\delta C_{2,\mathrm{ep}}$ (cyan) at time $t = 1.6$. Refer online version for interpretation of color.

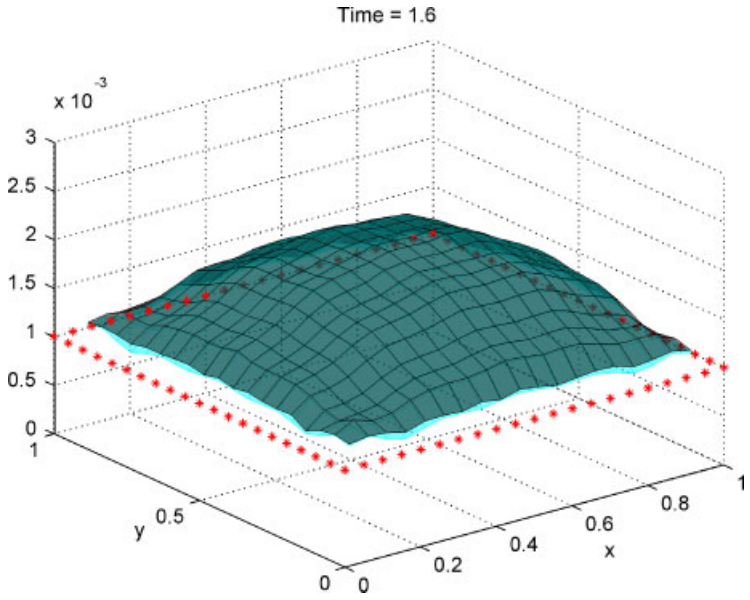

Figure 3. Maximum positive deviations in the controls δu (asterisks) and concentration fields (surface meshes) estimated by $\delta C_{2,\mathrm{ep}}$ (cyan) and $\delta \bar{C}_{2,\mathrm{w.c.}}$ computed by linear matrix inequalities (dark gray), which provides a tight upper bound, at time $t = 1.6$. Refer online version for interpretation of color.

DOI: 10.1002/oca

To assess the accuracy of the series expansions, and hence their suitability for use in robustness analysis, the worst-case deviations over the extreme points of the uncertainty set for each fixed (x, y, t) in the field were computed for the PDE (51) and the first-order (8) and second-order (15) expansions:

$$\delta C_{\mathrm{ep}} = \max_{\delta\hat{\lambda}_i \in \{\delta\underline{\lambda}_i, \delta\bar{\lambda}_i\}} |C(\hat{\lambda}_{\mathrm{nom}} + \delta\hat{\lambda}) - C(\hat{\lambda}_{\mathrm{nom}})|, \tag{72}$$

$$\delta C_{1,\mathrm{ep}} = \max_{\delta\hat{\lambda}_i \in \{\delta\underline{\lambda}_i, \delta\bar{\lambda}_i\}} |M\delta\hat{\lambda}|, \tag{73}$$

$$\delta C_{2,\mathrm{ep}} = \max_{\delta\hat{\lambda}_i \in \{\delta\underline{\lambda}_i, \delta\bar{\lambda}_i\}} |M\delta\hat{\lambda} + \delta\hat{\lambda}^{\mathrm{T}} H \delta\hat{\lambda}|, \tag{74}$$

$$\delta\bar{C}_{2,\mathrm{w.c.}} = \max_{\delta\underline{\lambda} \leqslant \delta\hat{\lambda} \leqslant \delta\bar{\lambda}} M\delta\hat{\lambda} + \delta\hat{\lambda}^{\mathrm{T}} H \delta\hat{\lambda}, \tag{75}$$

$$\delta\underline{C}_{2,\mathrm{w.c.}} = \min_{\delta\underline{\lambda} \leqslant \delta\hat{\lambda} \leqslant \delta\bar{\lambda}} M\delta\hat{\lambda} + \delta\hat{\lambda}^{\mathrm{T}} H \delta\hat{\lambda}, \tag{76}$$

where the subscript 'ep' denotes that this optimization is over the extreme points, and tight upper and lower bounds on (75) and (76) were obtained using the LMI and power iteration options, respectively, in the 'mussv' command in the Matlab Robust Control Toolbox [28]. The worst-case maximum deviations in the field due to uncertainties are not spatially uniform across the surface (see Figure 2). The effects of the uncertainties are significant, with

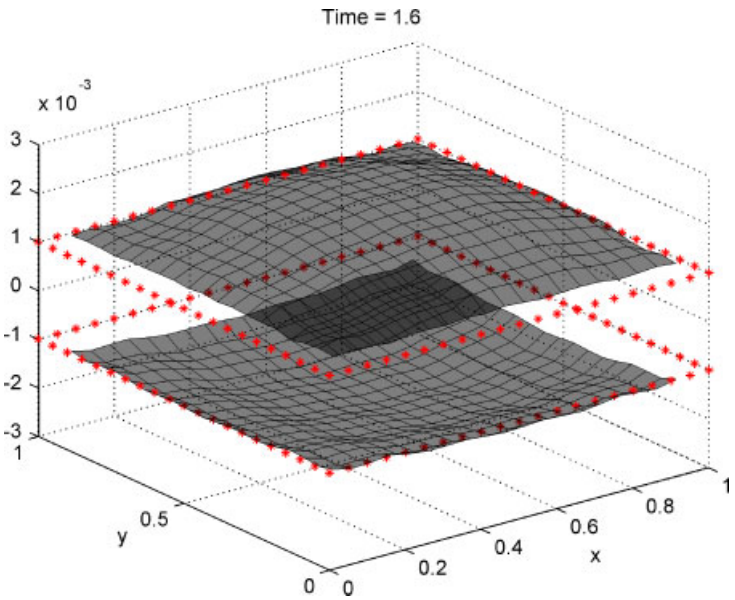

Figure 4. Maximum positive and negative deviations in the controls δu (asterisks) and concentration fields ($\delta\bar{C}_{2,\mathrm{w.c.}}$ and $\delta\underline{C}_{2,\mathrm{w.c.}}$) estimated by linear matrix inequalities (dark gray meshes), at time $t = 1.6$. The average difference of the absolute values (i.e., $\delta\bar{C}_{2,\mathrm{w.c.}} + \delta\underline{C}_{2,\mathrm{w.c.}}$) at each location is -5.1310×10^{-5}, indicating asymmetry of the uncertainty region about the $\delta C = 0$ plane. The maximum absolute difference is 1.6024×10^{-4}, which is about 16% of the space between consecutive horizontal dashed lines.

DOI: 10.1002/oca

the worst-case deviation being $> 10\%$ of the nominal value of the field for some times and spatial positions. The uncertainties in the dimensionless diffusivity and reaction rate constant do not affect the worst-case deviations on the boundaries of the spatial domain, since the values of the field on the boundaries are specified by the boundary control inputs marked by asterisks in Figure 2. The worst-case deviations of the concentration field at the boundaries are equal to the worst-case perturbations of the boundary control inputs, and those perturbations are felt uniformly throughout the spatial domain, as would be expected based on physical considerations.

The worst-case maximum deviations in the concentration fields computed for the second-order polynomial expansion are shown in Figure 3. The closeness of the concentration field computed from the LMI upper bound with that evaluated at the extreme points, which provides a lower bound on the worst-case perturbation, indicates that the LMI upper bound is a very accurate quantification of the worst-case perturbation based on the second-order expansion. Since the true worst-case concentration field based on the second-order expansion must be between the two concentration fields in Figure 3, the small differences between the concentration fields in Figure 3 provide an upper bound on the conservatism introduced by using LMIs for the robustness analysis.

The maximum and minimum perturbations in the concentration fields based on the second-order expansion, $\delta\bar{C}_{2,\text{w.c.}}$ and $\delta\underline{C}_{2,\text{w.c.}}$, computed using LMIs are shown in Figure 4. Based on the tight upper bounds on the worst-case perturbations in the concentration fields, the maximum and minimum deviations in the concentration fields are very similar in magnitude, but are not quite the same. There is some asymmetry of the uncertainty region for the concentration fields, which is not surprising as the concentration field depends nonlinearly on the dimensionless diffusion coefficient and reaction rate constant.

The polynomial-time upper and lower bounds for the most positive and most negative deviations of the second-order expansion computed by LMIs and power iteration are plotted in Figures 5 and 6. The average difference

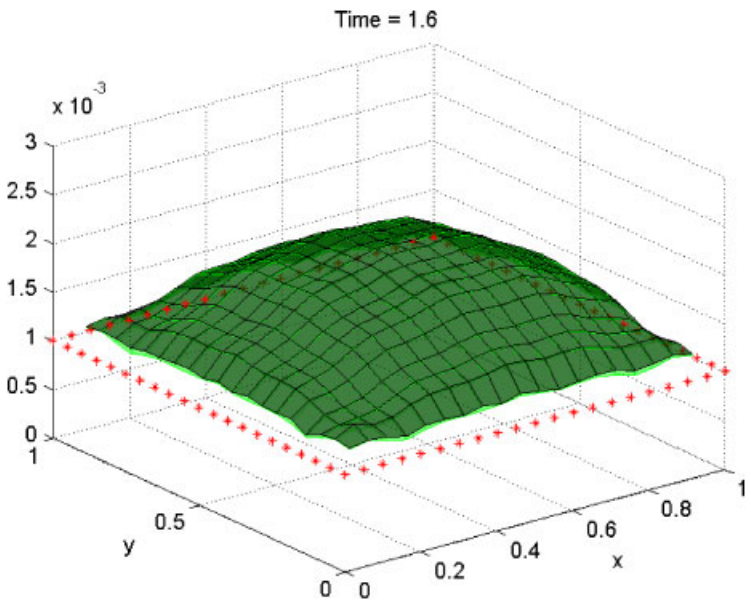

Figure 5. Maximum positive deviations in the controls δu (asterisks), and upper bound (dark green mesh) and lower bound (light green mesh) for the maximum positive deviations for the second-order expansion of the concentration field ($\delta\bar{C}_{2,\text{w.c.}}$). The average difference between the upper and lower bounds at each location is 9.4803×10^{-6} and the maximum absolute difference is 5.8634×10^{-5}. Refer online version for interpretation of color.

DOI: 10.1002/oca

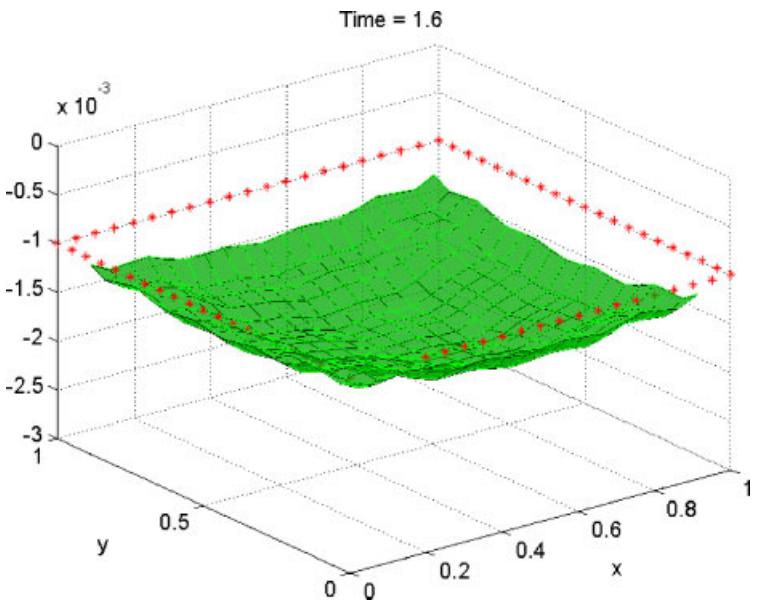

Figure 6. Most negative deviations in the controls δu (asterisks) and upper bound (dark green mesh) and lower bound (light green mesh) for the most negative deviations for the second-order expansion of the concentration field ($\delta \underline{C}_{2,\text{w.c.}}$). The average difference between the upper and lower bounds at each location is 4.8051×10^{-6} and the maximum absolute difference is 1.6487×10^{-5}. Refer online version for interpretation of color.

between the upper and lower bounds is $< 10^{-5}$, which is less than three orders-of-magnitude lower than the magnitude of the perturbations, which is $> 10^{-3}$. The average relative difference in the upper and lower bounds is less than 1% of the deviation in the concentration fields. The maximum relative difference between the upper and lower bounds is about 6%, which can be observed along the edges of the surfaces shown in Figure 5. The polynomial-time upper and lower bounds are 2 to 3 times tighter for computation of the most negative deviations than for the most positive deviations.

The effects of uncertainties significantly vary over time, with the first- and second-order expansions closely tracking the perturbed concentration fields (see Figure 7). The second-order expansion is much more accurate than the first-order expansion for the spatial average and at $(x, y) = (\frac{1}{4}, \frac{1}{4})$, but not significantly more accurate for $(x, y) = (\frac{1}{2}, \frac{1}{2})$. The expansions have an error of $\sim 10^{-4}$ for much of the spatial domain. For the entire time period, the polynomial-time LMI upper bound for the second-order expansion is very close to the lower bound obtained by evaluating the concentration field at the vertices of the uncertainty set (see Figure 7).

6. CONCLUSIONS

Methods are presented for the worst-case analysis of the effects of uncertainties on boundary control problems for finite-time DPSs that utilize low-order approximation of the mapping from uncertainties to output. Upper and lower bounds on the worst-case perturbations for each level of approximation are computed in polynomial-time by power iteration or LMIs. For a two-dimensional problem involving simultaneous reaction and diffusion, the worst-case estimates obtained by first- and second-order expansions were very close to the worst-case estimates computed by

DOI: 10.1002/oca

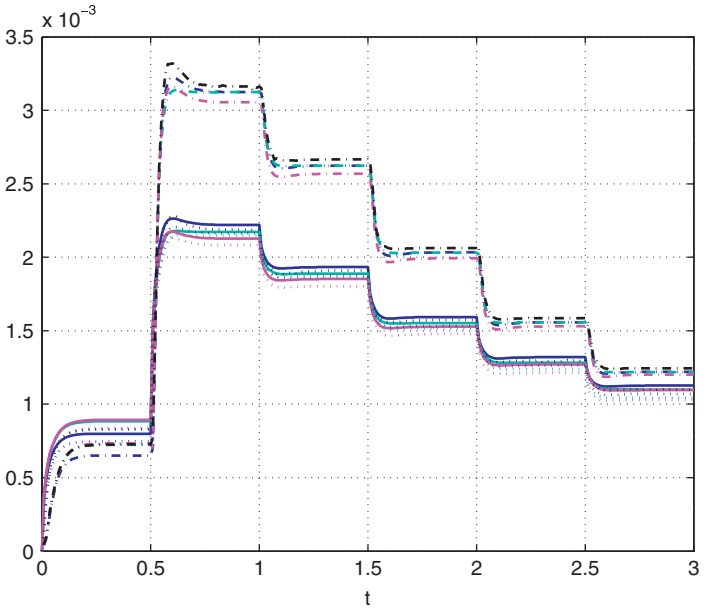

Figure 7. Maximum deviations in the field values due to uncertainties estimated by δC_{ep} (magenta), $\delta C_{1,\mathrm{ep}}$ (blue), and $\delta C_{2,\mathrm{ep}}$ (cyan), averaged over the spatial domain (-), and δC_{ep} (magenta), $\delta C_{1,\mathrm{ep}}$ (blue), $\delta C_{2,\mathrm{ep}}$ (cyan), and $\max\{\delta \bar{C}_{2,\mathrm{w.c.}}, -\delta \underline{C}_{2,\mathrm{w.c.}}\}$ (black, as computed from the LMI upper bound using 'mussv') at $(x, y) = (\frac{1}{2}, \frac{1}{2})$ (-·) and $(x, y) = (\frac{1}{4}, \frac{1}{4})$ (···). Refer online version for interpretation of color.

using the original system. On average the polynomial-time upper and lower bounds were within 1% of each other, with a maximum difference of about 6%. The relatively low computational cost of these polynomial-time analysis tools indicates the feasibility of their incorporation into numerical algorithms for the design of optimal boundary controls for finite-time DPSs to be robust to uncertainties in model parameters and control implementation.

ACKNOWLEDGEMENTS

Partial support for this research was provided by grants from the the Institute for Advanced Computing Applications and Technologies, the National Science Foundation (Grant Number 0828123), and the National Institute of Biomedical Imaging and Bioengineering, National Institutes of Health. A preliminary version of this manuscript was presented at the Eighteenth International Symposium on Mathematical Theory of Networks and Systems [1].

REFERENCES

1. Kishida M, Braatz RD. Robustness analysis of distributed parameter systems with application to the 2D reaction–diffusion equation. *Proceedings of the 18th International Symposium on Mathematical Theory of Networks and Systems*, Blacksburg, VA, 2008; SSRussell1.4.
2. Boskovic DM, Krstic M, Liu WJ. Boundary control of an unstable heat equation via measurement of domain-averaged temperature. *IEEE Transactions on Automatic Control* 2001; **46**:2022–2028.
3. Liu WJ. Boundary feedback stabilization of an unstable heat equation. *SIAM Journal on Control and Optimization* 2003; **42**:1033–1043.
4. Bleris LG, Kothare MV. Reduced order distributed boundary control of thermal transients in microsystems. *IEEE Transactions on Control Systems Technology* 2005; **13**:853–867.

DOI: 10.1002/oca

5. Kishida M, Pack DW, Braatz RD. State-constrained optimal spatial field control for controlled release in tissue engineering. *Proceedings of the American Control Conference*, 2010; 4361–4366.
6. Lang J. Adaptive computation for boundary control of radiative heat transfer in glass. *Journal of Computational and Applied Mathematics* 2005; **183**:312–326.
7. Boyd S, El Ghaoul L, Feron E, Balakrishnan V. *Linear Matrix Inequalities in System and Control Theory*. SIAM Press: Philadelphia, PA, 1997.
8. Dullerud GE, Paganini F. *A Course in Robust Control Theory*. Springer: New York, 2000.
9. Zhou K, Doyle JC, Glover K. *Robust and Optimal Control*. Prentice-Hall: Upper Saddle River, NJ, 1995.
10. Or AC, Speyer JL. Robust control for convection suppression in a fluid layer: the effects of boundary properties, actuator lag, and major parameter uncertainties. *Physical Review E* 2006; **73**:046307.
11. Poznyak AS, Palacios AR. Robust boundary control for linear time-varying infinite dimensional systems. *International Journal of Control* 1999; **72**:392–403.
12. Pan W, Tatang MA, McRae GJ, Prinn RG. Uncertainty analysis of indirect radiative forcing by anthropogenic sulfate aerosols. *Journal of Geophysical Research* 1998; **103**:3815–3823.
13. Ma DL, Braatz RD. Worst-case analysis of finite-time control policies. *IEEE Transactions on Control Systems Technology* 2001; **9**:766–774.
14. Nagy ZK, Braatz RD. Worst-case sand distributional robustness analysis of finite-time control trajectories for nonlinear distributed parameter systems. *IEEE Transactions on Control Systems Technology* 2003; **11**:494–504.
15. Nagy ZK, Braatz RD. Distributional uncertainty analysis using power series and polynomial chaos expansions. *Journal of Process Control* 2007; **17**:229–240.
16. Braatz RD, Young PM, Doyle JC, Morari M. Computational complexity of μ calculation. *IEEE Transactions on Automatic Control* 1994; **39**:1000–1002.
17. Braatz RD, Russell EL. Robustness margin computation for large scale systems. *Computers and Chemical Engineering* 1999; **23**:1021–1030.
18. Ferreres G, Fromion V. Computation of the robustness margin with the skewed μ tool. *Systems and Control Letters* 1997; **32**(4):193–202.
19. Newlin MP, Smith R. A generalization of the structure singular value and its application to model validation. *IEEE Transactions on Automatic Control* 1998; **43**(7):901–907.
20. Young PM, Doyle JC. A lower bound for the mixed μ problem. *IEEE Transactions on Automatic Control* 1997; **42**:123–128.
21. Russell EL, Power CPH, Braatz RD. Multidimensional realization of large scale uncertain systems for multivariable stability margin computation. *International Journal of Robust and Nonlinear Control* 1997; **7**:113–125.
22. Chen J, Fan MKH, Nett CN. Structured singular values and stability analysis of uncertain polynomials, part 1: the generalized mu. *Systems and Control Letters* 1994; **23**:53–65.
23. Loeblein C, Perkins JD. Structural design for on-line process optimization: I. Dynamic economics of MPC. *AIChE Journal* 1999; **45**:1018–1029.
24. Loeblein C, Perkins JD, Srinivasan B, Bonvin D. Performance analysis of on-line batch optimization systems. *Computers and Chemical Engineering* 1997; **21**:S867–S872.
25. Loeblein C, Perkins JD, Srinivasan B, Bonvin D. Economic performance analysis in the design of on-line batch optimization systems. *Journal of Process Control* 1999; **9**:61–78.
26. Glemmestad B, Skogestad S, Gundersen T. Optimal operation of heat exchanger networks. *Computers and Chemical Engineering* 1999; **23**(4–5):509–522.
27. Govatsmark MS, Skogestad S. Selection of controlled variables and robust setpoints. *Industrial and Engineering Chemistry Research* 2005; **44**:2207–2217.
28. Balas G, Chiang R, Packard A, Safonov M. *Robust Control Toolbox 3*: *User's Guide*. The Mathworks, Inc.: Natick, MA, 2010; Release 2010a.

DOI: 10.1002/oca